2014

Green luminescence in Mg-doped GaN

Michael A. Reshchikov
Virginia Commonwealth University, mreshchi@vcu.edu

Denis Demchenko
Virginia Commonwealth University, ddemchenko@vcu.edu

J. D. McNamara
Virginia Commonwealth University

S. Fernández-Garrido
Paul Drude Inst Festkorperlektron

R. Calarco
Paul Drude Inst Festkorperlektron

Green luminescence in Mg-doped GaN

M. A. Reshchikov,[1,*] D. O. Demchenko,[1] J. D. McNamara,[1] S. Fernández-Garrido,[2] and R. Calarco[2]

[1]*Department of Physics, Virginia Commonwealth University, Richmond, Virginia 23284, USA*

[2]*Paul-Drude-Institut für Festkörperelektronik, 10117 Berlin, Germany*

A majority of the point defects in GaN that are responsible for broad photoluminescence (PL) bands remain unidentified. One of them is the green luminescence band (GL2) having a maximum at 2.35 eV which was observed previously in undoped GaN grown by molecular-beam epitaxy in Ga-rich conditions. The same PL band was observed in Mg-doped GaN, also grown in very Ga-rich conditions. The unique properties of the GL2 band allowed us to reliably identify it in different samples. The best candidate for the defect which causes the GL2 band is a nitrogen vacancy (V_N). We propose that transitions of electrons from the conduction band to the $+/2+$ transition level of the V_N defect are responsible for the GL2 band in high-resistivity undoped and Mg-doped GaN.

PACS number(s): 71.55.Eq, 61.72.uj, 71.15.Mb

I. INTRODUCTION

A. Nitrogen vacancy in GaN

Achieving conductive and reliable *p*-type GaN is a challenging task, because doping with Mg (the only successful *p*-type dopant) produces some native donors due to the self-compensation effect [1]. Understanding and explaining the properties of point defects in this material is crucial for improving the efficiency and longevity of GaN-based light-emitting devices. One of the native defects in Mg-doped GaN is the nitrogen vacancy (V_N).

The V_N defect is predicted to have a low formation energy in *p*-type GaN, especially when it is grown under Ga-rich conditions, where the supply of Ga exceeds that of N. According to recent calculations by Yan *et al.* [2], the V_N defect in *p*-type or high-resistivity GaN is a negative-*U* defect, with the thermodynamic $+/3+$ level at 0.47 eV above the valence band. Unfortunately, these authors did not provide any information about the energy positions of the $2+/3+$ and $+/2+$ transition levels, which can be revealed through experiments. However, they calculated that the expected zero-phonon line (ZPL), E_0, and the maximum of the luminescence band, $\hbar\omega_{max}$, caused by transitions of electrons from the conduction band to the $2+/3+$ level of the V_N defect are 2.99 and 2.18 eV, respectively, and suggested that a yellow luminescence (YL) band can be observed in this case [2]. Alkauskas *et al.* [3] calculated the line shape for this luminescence band by mapping a multidimensional vibrational problem onto an effective one-dimensional configuration-coordinate diagram. They predicted that the full width at half maximum (FWHM) of the V_N-related luminescence band at low temperature, $W(0)$, is 0.33 eV. These data were compared with the YL band observed by Salviati *et al.* [4] in Mg-doped GaN [$\hbar\omega_{max} \approx 2.2$ eV, $W(0) \approx 0.4$ eV]. Note that the authors of Ref. [4] attributed the YL band to transitions from the deep N_{Ga} donor to the shallow Mg_{Ga} acceptor, although, in our opinion, the arguments of such an attribution are not convincing.

Alkauskas *et al.* [3] have also predicted that the dominant phonon energy $\hbar\Omega$ of the ground and excited states of the

V_N defect (with charges $3+$ and $2+$, respectively) were $\hbar\Omega_g = 23 \pm 2$ meV and $\hbar\Omega_e = 21 \pm 3$ meV. Finally, the Huang-Rhys factor, S, for the ground and excited states are calculated to be $S_g = 36.0$ and $S_e = 34.8$, respectively [3]. The Huang-Rhys factor is a measure of the electron-phonon coupling, and is represented by the average number of emitted or absorbed phonons accompanying an optical transition. Such large values of S_g and S_e indicate a very strong electron-phonon coupling for the V_N defect. It is instructive to compare the above-calculated parameters with the following experimentally found ranges of parameters for the YL band in GaN [$\hbar\omega_{max} = 2.13-2.25$ eV, $W(0) = 0.38-0.43$ eV, $E_0 = 2.6-2.7$ eV, $\hbar\Omega_g = 40-51$ meV, $\hbar\Omega_e = 41-52$ meV, $S_a = 10.2-13.4$, and $S_e = 10.3-12.8$] [5]. While the position and width of the YL band agree with the predicted values for the luminescence band caused by transitions of electrons from the conduction band to the $3+$ level of the V_N defect, the vibrational parameters for the YL-related defect and for the V_N center look very different. In this work, we demonstrate that a much better candidate for photoluminescence (PL) created by the V_N defect is the green luminescence band GL2 having a maximum at 2.35 eV [5]. As shown below, the GL2 band is observed in both Mg-doped and undoped GaN samples; however, Mg content is only responsible for the position of the Fermi energy and not for the GL2 band itself.

B. Green luminescence band in undoped high-resistivity GaN

Usually, undoped GaN produces the YL band with a maximum at 2.2 eV [5]. However, when GaN is grown by the molecular-beam epitaxy (MBE) method in extremely Ga-rich conditions, the resulting samples become high resistivity, and the PL spectrum shows a green luminescence band with a maximum at 2.35 eV, labeled GL2 in Ref. [5]. It should not be confused with the green luminescence (GL) band observed in high-quality, undoped GaN grown by hydride vapor phase epitaxy (HVPE) [5]. In some of the high-resistivity samples, the GL2 band is the dominant PL band, with a quantum efficiency of up to 1%. The FWHM of the GL2 band is 0.22–0.25 eV, which is much smaller than the value for the YL band. With increasing excitation intensity from 10^{-4} to 100 W/cm^2 at 18 K, the position of the GL2 band

*mreshchi@vcu.edu

does not change, but its quantum efficiency decreases by two orders of magnitude, presumably due to the saturation of the related defect with photogenerated holes. In contrast to a majority of PL bands in undoped GaN, the intensity of the GL2 band decays exponentially after a pulsed excitation, even at low temperatures (15–100 K), with a characteristic PL lifetime of about 250 μs. With increasing temperature, the intensity of the GL2 band is constant up to $\sim$100 K. At higher temperatures, thermal quenching of the PL is observed, revealing an activation energy of 120 ± 20 meV. Above 200 K, the GL2 band becomes masked by other PL bands. The GL2 band maximum shifts to higher energy by about 10–30 meV as the temperature increases from 15 to 200 K. The temperature dependence of the GL2 band FWHM, $W(T)$, follows the law expected for defects with strong electron-phonon coupling [5],

$$W(T) = W(0)\sqrt{\coth\left(\frac{\hbar\Omega_e}{2kT}\right)},\qquad(1)$$

where k is Boltzmann's constant and $\hbar\Omega_e$ is the energy of the dominant phonon mode for the defect in the excited state. By fitting the experimental data with Eq. (1), $\hbar\Omega_e$ was estimated to be 23 meV. This value is much smaller than the dominant phonon energies for acceptors responsible for several PL bands in GaN, which range from 40 to 50 meV [5]. Assuming that adiabatic potentials in the ground and excited states are similar (i.e., $\hbar\Omega_g = \hbar\Omega_e$ and $S_g = S_e$), the Huang-Rhys factors for the defect responsible for the GL2 band were estimated to be about 20. This value is much larger than the typical values for other defects in GaN, which range from 3 to 10 (Ref. [5]), suggesting a different origin of the GL2 band.

In contrast to other PL bands in GaN, the GL2 band could not be excited with photon energies below the band gap [6]. This finding may indicate that the characteristic PL excitation band for the GL2 band lies at energies higher than the band gap. The GL2 band was attributed to an internal transition in some defect having very strong electron-phonon coupling [5]. The PL quenching at temperatures above 100 K was explained by a conversion of the defect from a radiative state to a nonradiative state due to phonon-assisted transitions from an excited state to the ground state via crossed adiabatic potentials—the so-called Seitz-Mott mechanism [7]. This conclusion was based on the fact that the activation energy of the thermal quenching ($\sim$0.1 eV) was too small for a defect causing a PL band in the green region of the spectrum. In Secs. IV A and IV D, we suggest a different mechanism for the PL quenching, which agrees with all the available experimental data. As for the identification of the defect responsible for the GL2 band, it is most likely a native defect (or a complex) related to the excess of Ga, because the samples were undoped. Since such samples were high resistivity, it was originally proposed that a good candidate for the GL2 defect is the gallium antisite (Ga$_N$) [5]. However, from first-principles calculations, the formation of the Ga$_N$ defect is very unlikely if the Fermi level is far from the valence band [1]. In this work, we present evidence that the nitrogen vacancy is the most likely candidate for the defect responsible for the GL2 band.

II. METHODS

A. Experimental details

The samples studied in this work were 750–800-nm-thick GaN:Mg layers grown in a custom-built MBE system equipped with a radio-frequency N_2 plasma source for active N, and solid-source effusion cells for Ga and Mg. All samples were prepared on top of 5–6-μm-thick undoped GaN(0001) templates grown by HVPE on 2-in. sapphire substrates. The GaN:Mg layers were grown at $T = 690$ °C under Ga-rich conditions [8,9], using a Ga/N flux ratio of 1.4. The growth rate, determined by the impinging active N flux, was 0.5 μm/h. The Mg concentration was varied by changing the Mg flux. The Mg cell temperatures and the corresponding beam equivalent pressures used in this work were in the ranges of 420–440 °C and 0.5 to 1×10^{-8} mbar, respectively. The concentration of free holes, p, and their mobility, μ, were estimated from the analysis of room-temperature Hall-effect data to be $\sim 1 \times 10^{18}$ cm^{-3} and ~ 10 cm^2/V s, respectively. The concentration of Mg atoms was estimated to be 2 to 5×10^{19} cm^{-3} from secondary ion mass spectrometry (SIMS) measurements on GaN:Mg layers grown in identical conditions. The residual concentrations of O and Si, as measured by SIMS from comparable but nonintentionally doped GaN layers, were below 5×10^{16} cm^{-3}. There was no postgrowth annealing, except for the samples used for the Hall-effect measurements which were annealed for 10 min at 480 °C to improve the p-type contacts.

Steady-state PL was excited with a continuous-wave He-Cd laser (40 mW). Other details of the PL measurements can be found in Ref. [10]. The absolute internal quantum efficiency of PL, η, is defined as $\eta = I^{\text{PL}}/G$, where I^{PL} is the integrated PL intensity from a particular PL band and G is the concentration of electron-hole pairs created by the laser per second in the same volume. To find η, we compared the integrated intensity of the ultraviolet luminescence (UVL) band with the PL intensity obtained from a calibrated GaN sample [10,11]. All of the measurements were done under identical conditions with calibrated excitation power density P_{exc}.

B. Theoretical details

In order to identify the microscopic origin of the observed GL2 band, we performed Heyd-Scuseria-Ernzerhof (HSE) hybrid functional [12] calculations of several possible defect configurations. In the HSE hybrid functional, as implemented in the VASP program [13], we adjusted the fraction of exact exchange to 0.312 and the screening parameter to 0.2 Å^{-1}. It has been shown that these parameters accurately reproduce energetics and optical properties of defects in GaN [14]. The computed band gap of 3.5 eV agrees with the low-temperature experimental value of 3.50 eV, and computed relaxed lattice parameters for wurtzite GaN ($a = 3.210$ Å, $c = 5.198$ Å, and $u = 0.377$) also agree with experimental values ($a = 3.189$ Å, and $c = 5.185$ Å) [15]. The 128-atom supercells were used with all internal degrees of freedom relaxed using HSE hybrid functional calculations to result in forces of 0.05 eV/Å or less. The plane-wave basis sets with a 400 eV cutoff at the Γ point were used in all calculations. Spin polarized calculations were performed in all cases. The defect

formation energy is defined as the total energy difference of the supercell including the defect and the bulk supercell, compensating for the difference in the chemical potentials of the missing (added) atoms in the defect cell, and adding the charging energy of a defect for nonzero charge states. The chemical potentials for N, Ga, and Mg are obtained from HSE calculations of the N_2 molecule, metallic Ga, and Mg_3N_2, respectively. Several corrections to the formation energies of defects due to several physical origins [16] are applied as described elsewhere [14,17]. Note that comparing the absolute values of the computed formation energies to the expected experimental concentrations of defects should be done with caution. Since the conditions in the MBE growth are far from thermal equilibrium, direct comparisons are not appropriate. Nevertheless, we expect to capture energetic trends for varying Fermi energies in different samples, which is useful for the analysis of possible trends in defect concentrations and sample compensation effects. Most importantly, formation energy differences or the intersections of the formation energy lines (i.e., thermodynamic transition levels) are well represented by theory—regardless of the sample growth conditions. The same holds for the computed optical transitions. This allows for the direct comparison of the theoretical calculations with experimental data and the identification of defects responsible for specific PL bands.

III. RESULTS

A. Two regions with different optical properties

The optical properties of Mg-doped GaN varied greatly even across the same wafer. For each wafer, we could find regions (typically closer to the edge of the 2-in. wafer) which emit bright green light and regions (typically near the wafer center) which emit violet light when illuminated with UV light. Surprisingly, the boundary between the two regions ("green" and "violet") was very sharp. Typical PL spectra from the green and violet regions at room temperature are shown in Fig. 1. The intensity of the green luminescence band, which has a maximum at 2.38 eV at room temperature (this is the GL2 band as will be shown below), is stronger by two orders of magnitude in the green region. The violet color of the violet region originates from a strong UVL band which has a maximum at 3.26 eV. The intensity of the UVL band in the green region is lower by at least two to three orders of magnitude. The near-band-edge (NBE) peak at 3.39 eV is relatively strong only in the violet region. Figure 2 shows the changes in the GL2 and UVL intensities when a laser beam passes through the sharp boundary between the green and violet regions of one of the samples. Across the boundary between the regions (about 2 mm), the intensities of the GL2 and UVL bands change by about two orders of magnitude in opposite directions. It is interesting that, in addition to the sharp boundary separating the green and violet regions, small spots with sizes of about 0.2 mm can be found (a feature at 8.5 mm in Fig. 2) where the intensities of the GL2 and UVL bands abruptly change.

Hot-probe measurements indicated good p-type conductivity in the violet regions, while the results for the green regions were inconclusive. Although p-type conductivity was obtained
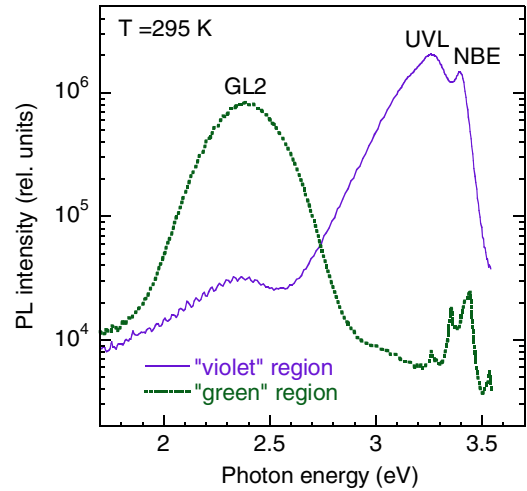

FIG. 1. (Color online) PL spectra from the green and violet regions of the 12×12 mm sample M9599 at room temperature with $P_{exc} = 0.2$ W/cm^2. The weak oscillations with a period of about 30–40 meV are due to a Fabry-Perot effect in the sapphire/GaN/air cavity, revealing the total thickness of the GaN layers to be about 7 μm.

from the Hall-effect measurements for all samples, the 12×12 mm samples in these experiments contained mostly violet regions which probably dominated the electrical conductivity. Based on the hot-probe measurements and PL data obtained in this work, we predict that the green regions are semi-insulating.

B. Effect of the excitation intensity on the GL2 band

The low-temperature PL spectra from the green region at several excitation intensities are shown in Fig. 3. The NBE emission is weak, and its main peak at 3.467 eV can be attributed to an exciton bound to either a shallow donor or a shallow acceptor. The exciton emission intensity increases superlinearly with the excitation intensity, which is typical for
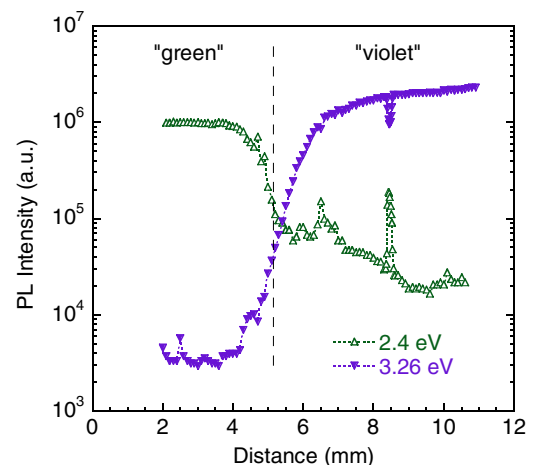

FIG. 2. (Color online) PL peak intensity for the GL2 (at 2.4 eV) and UVL (at 3.26 eV) bands as a function of the laser beam location on the sample surface while crossing the boundary between the green and violet regions. Sample M9599. $T = 295$ K, $P_{exc} = 0.2$ W/cm^2.
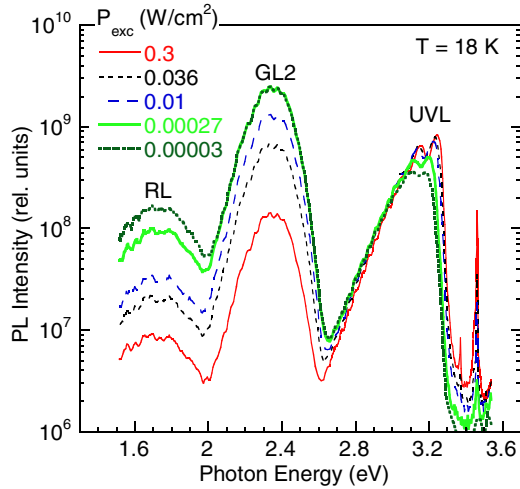
FIG. 3. (Color online) PL spectrum from Mg-doped GaN (the green region of sample 9591) at $T = 18$ K and selected excitation power densities. Each PL spectrum is divided by the corresponding P_{exc}.

p-type or high-resistivity GaN samples. In the visible portion of the spectra, three defect-related PL bands can be seen: the UVL band with a main peak at about 3.25 eV, the GL2 band with a maximum at 2.35 eV, and a red luminescence (RL) band with a maximum at 1.73 eV. With decreasing excitation intensity, the fine structure of the UVL band becomes less resolved, and the band shifts to lower photon energies, which can be explained by the presence of potential fluctuations in heavily doped or high-resistivity GaN:Mg [18]. Interestingly, the GL2 band does not shift with excitation intensity, and its shape remains intact, which will be explained in Sec. IV B.

The intensity of both the GL2 band and RL band increases sublinearly with excitation intensity, while the UVL band increases slightly superlinearly. In the limit of low excitation intensities, the quantum efficiency, η, of the RL, GL2, and UVL bands in the green region was estimated as 1%, 7%, and 1%, respectively, while these values for the violet region at 18 K were typically much lower (about 0.01%, 0.1%, and 0.1%, respectively). The dependence of η on the excitation intensity for the GL2 band in the green region is shown in Fig. 4. We can see that for low excitation intensities, η is independent of the excitation intensity, and for $P_{exc} > 10^{-3}$ W/cm^2, the quantum efficiency decreases. The dependence is fit with the following expression [19,20]:

$$\eta = \frac{N}{\alpha \tau P_0} \ln\left(1 + \frac{\alpha \tau P_0 \eta_0}{N}\right). \qquad (2)$$

Here, P_0 is the excitation intensity (expressed as the number of photons passing through a unit area of the sample surface per unit time), N is the concentration of defects responsible for the GL2 band, η_0 is the quantum efficiency of the GL2 band in the limit of low excitation intensities, τ is the PL lifetime, and α is the absorption coefficient [$\alpha \approx 1.2 \times 10^5$ cm^{-1} for GaN at 3.81 eV (Ref. [21])]. The PL lifetime at 18 K was found to be 300 μs from time-resolved PL measurements. The only fitting parameter in Eq. (2) is N. From the best fit, we have found that $N = 10^{16}$ cm^{-3}.
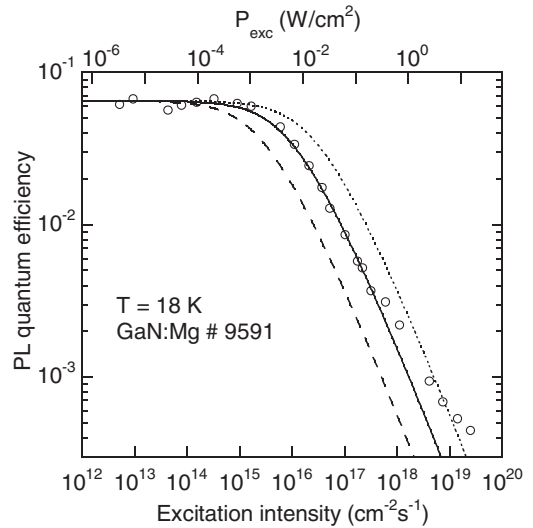

FIG. 4. Dependence of PL quantum efficiency on excitation intensity for the GL2 band at 18 K. Sample 9591 (green region). The solid line is calculated by using Eq. (2) with the following parameters: $N = 1 \times 10^{16}$ cm^{-3}, $\tau = 300$ μs, $\eta_0 = 0.065$, and $\alpha = 1.2 \times 10^5$ cm^{-1}. The dashed and dotted lines are calculated with $N = 3 \times 10^{15}$ cm^{-3} and $N = 3 \times 10^{16}$ cm^{-3}, respectively.

C. Effect of temperature on the GL2 band

At 18 K, the GL2 band in several GaN:Mg samples has a maximum at 2.350 $\pm$ 0.005 eV, and its FWHM is 230 $\pm$ 5 meV. With increasing temperature from 18 to 300 K, the GL2 band shifts to higher energies by about 30 meV, and its width increases. The temperature dependence of its normalized FWHM is shown in Fig. 5. From the fit of this dependence with Eq. (1), we find $\hbar\Omega_e = 23 \pm 1$ meV (Fig. 5)—exactly the same value as that for the GL2 band in undoped GaN grown in very Ga-rich conditions [5]. This strongly suggests that in both
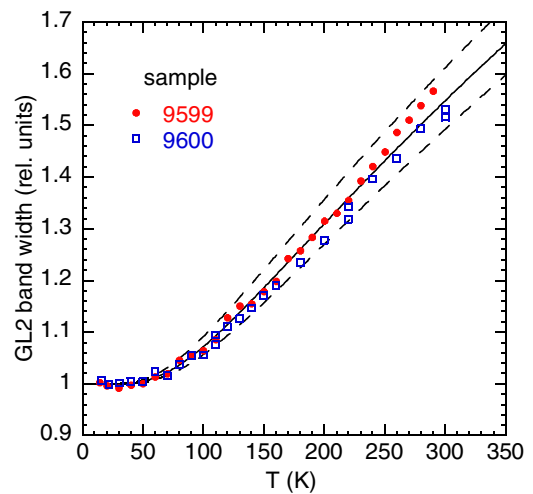

FIG. 5. (Color online) Temperature dependence of the GL2 bandwidth, normalized to the lowest temperature. Solid line is calculated by using Eq. (1) with $\hbar\Omega_e = 23$ meV. Dashed lines are calculated using Eq. (1) with $\hbar\Omega_e = 21$ meV (top line) and $\hbar\Omega_e = 25$ meV (bottom line).

Mg-doped and undoped high-resistivity GaN, the GL2 band is caused by the same defect, which implies that the defect is not related to Mg.

The intensity of the GL2 band is independent of temperature up to 100 K. The PL quantum efficiency in the temperature range between 100 and 170 K decreases and can be fit with the following expression:

$$\eta(T) = \frac{\eta_0}{1 + C\,\exp(-E_A/kT)}, \qquad (3)$$

where C is a constant and E_A is customarily explained as some activation energy. At higher temperatures, an abrupt quenching of the GL2 band is observed. The slope of this dependence in the Arrhenius plot is about 650 meV (Fig. 6).

The transition from the weakly temperature-dependent part (with $E_A = 110$ meV) to the abrupt quenching (with $E_A \approx 650$ meV) occurs at a characteristic temperature T_0 (Fig. 6). Interestingly, T_0 shifts to higher temperatures with increasing excitation intensity, demonstrating a classical case of abrupt and tunable thermal quenching of PL [7,10,22]. When $1/T_0$ is plotted as a function of the logarithm of excitation intensity, a straight line is obtained (Fig. 7).

This behavior can be explained by a phenomenological model for a high-resistivity or p-type semiconductor with three types of defects (a shallow donor, a radiative center, and a dominant nonradiative center) [7,10]. In this model, T_0 is the temperature at which the concentration of thermally emitted holes becomes equal to the concentration of optically generated holes. Its dependence on excitation power can be

FIG. 7. (Color online) The dependence of the critical temperature T_0 on the excitation intensity for the green region of sample 9599. The solid line is calculated by using Eq. (4) with $B = 3 \times 10^{31}$ cm^{-3} s^{-1} and $E_A = 460$ meV.

described with the following expression:

$$T_0 = \frac{E_A/k}{\ln(B/G)}, \qquad (4)$$

where E_A is the ionization energy of the radiative center responsible for the PL, G is the electron-hole generation rate, and B is a sample-dependent factor:

$$B = \frac{C_{pS}N_S(N_A - N_D)N_v}{gN_D}. \qquad (5)$$

Here, N_S and C_{pS} are the concentration of the nonradiative centers and their hole-capture coefficient, respectively; N_A and N_D are the concentrations of the radiative defect and the shallow donor, respectively; N_v is the effective density of states in the valence band; and g is the degeneracy of the radiative defect level (assumed to be equal to 2). From the fit of the experimental data with Eq. (4), we find $E_A = 0.46$ eV. When the weak temperature dependence of N_v is accounted for in this fit, the ionization energy is adjusted to $E_A = 0.43 \pm 0.03$, resulting in an undistinguishable fit. This value should be interpreted as the ionization energy of the GL2-related defect, and most probably the position of its level measured from the top of the valence band.

In the violet region, the thermal quenching of the GL2 and UVL bands (Fig. 8) was different from that in the green region. The intensity of the UVL band decreases very slowly with temperature, as was discussed in Ref. [23]. The absence of thermal quenching with the activation energy equal to the ionization energy of the Mg$_{Ga}$ acceptor (0.2 eV) is consistent with p-type conductivity in the violet region. Indeed, the concentration of additional (photogenerated) holes bound to acceptors is insignificant in comparison with the equilibrium (dark) concentration of bound holes for temperatures up to room temperature in p-type GaN. Therefore, the intensity of the UVL band, which is proportional to the concentration of bound holes and free electrons, is expected to be nearly
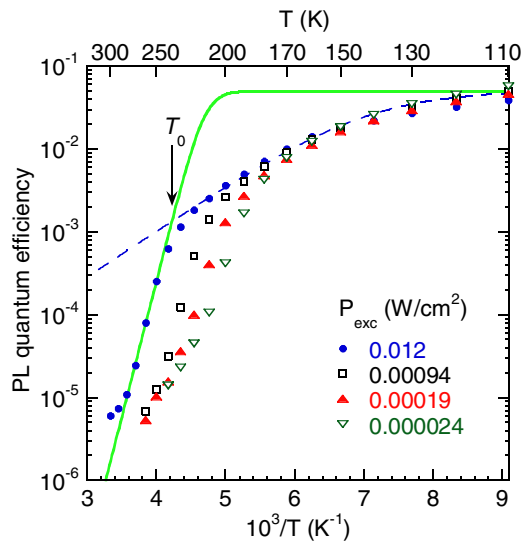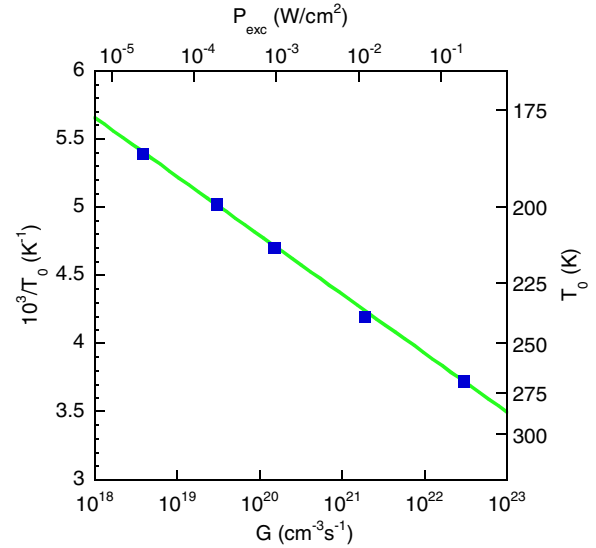

FIG. 6. (Color online) Temperature dependence of the PL quantum efficiency for the GL2 band at selected excitation power densities in the green region of sample M9599. The dashed line is calculated by using Eq. (3) with $E_A = 110$ meV and $C = 8 \times 10^3$. The solid line is calculated by using Eq. (3) with $E_A = 650$ meV and $C = 2.5 \times 10^{15}$. An arrow indicates the critical temperature T_0 for $P_{exc} = 0.012$ W/cm^2, at which the parts of the dependence with different slopes intersect when extrapolated.
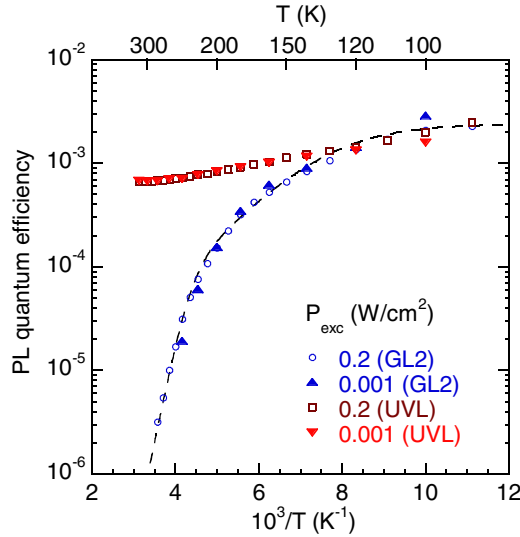
FIG. 8. (Color online) Temperature dependence of the quantum efficiency for the GL2 and UVL bands at two excitation power densities in the violet region of sample M9599. The dashed line is calculated by using Eq. (6) with $E_{A1} = 80$ meV, $C_1 = 1.2 \times 10^3$, $E_{A2} = 400$ meV and $C_2 = 1.3 \times 10^{10}$.

independent of temperature. This is in contrast to conductive *n*-type GaN where the thermal emission of photogenerated bound holes to the valence band leads to PL quenching with an activation energy of $\sim$0.2 eV, which is the Mg acceptor ionization energy [5].

The temperature dependence of the quantum efficiency of the GL2 band in the violet region shows two slopes and can be described with the following expression (Fig. 8):

$$\eta(T) = \frac{\eta_0}{1 + C_1 \exp(-E_{A1}/kT) + C_2 \exp(-E_{A2}/kT)}, \quad (6)$$

where C_1 and C_2 are constants, and E_{A1} and E_{A2} are the activation energies of the thermal quenching for temperatures in the ranges between 100 and 200 K and above 200 K, respectively. The quenching behavior in the range of 100–200 K is similar to that in the green region. However, the quenching at temperatures above 200 K is less abrupt ($E_A \approx 0.4$ eV) and not tunable.

D. Shape of the GL2 band

The normalized spectrum of the GL2 band at 18 K for three samples is shown in Fig. 9. The shape of the GL2 band is almost symmetrical, and in the first approximation it can be described with a Gaussian function (the dashed curve in Fig. 9):

$$I^{PL} \propto \exp\left(-\frac{(\hbar\omega - \hbar\omega_{\max})^2}{2\sigma^2}\right), \quad (7)$$

where $\hbar\omega$ is the photon energy, $\hbar\omega_{\max}$ is the position of the GL2 band maximum, and the parameter σ describes the bandwidth (FWHM = $\sqrt{8\ln 2}\sigma$). A better fit (the solid red line in Fig. 9) accounts for a slight asymmetry of the PL band and can be obtained by using the following empirical
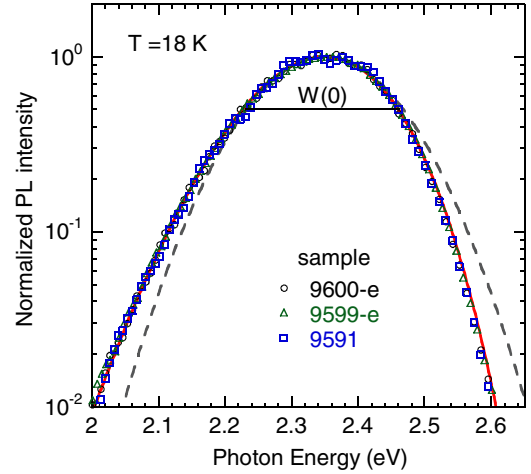

FIG. 9. (Color online) PL spectrum of the GL2 band for three samples at 18 K (the absolute intensity is normalized at the maximum). The FWHM of the GL2 band, $W(0)$, is indicated with a horizontal line. The dashed line is calculated by using Eq. (7) with $\hbar\omega_{\max} = 2.35$ eV and $\sigma = 0.1$ eV. The solid red line is calculated by using Eq. (8) with $\hbar\omega_{\max} = 2.35$ eV, $E_0 = 2.85$ eV, $\hbar\Omega_e = 23$ meV, and $S_e = 26.5$. In both fits, $W(0) = 230$ meV.

function, which is derived in the Appendix:

$$I^{PL} \propto \exp\left[-2S_e\left(\sqrt{\frac{E_0 + 0.5\hbar\Omega_e - \hbar\omega}{E_0 + 0.5\hbar\Omega_e - \hbar\omega_{\max}}} - 1\right)^2\right]. \quad (8)$$

In this fit, the width of the PL band was adjusted by varying the parameter S_e, and the degree of the asymmetry was adjusted by varying the parameter E_0, while parameters $\hbar\Omega_e$ and $\hbar\omega_{\max}$ were fixed. Note that the FWHM in both fits is the same [$W(0) = 230$ meV], and the asymmetry becomes evident only when the PL band is plotted in a logarithmic scale, when its intensity changes by two orders of magnitude. The value of the ZPL (E_0) is estimated to be in the range of 2.85–3.0 eV (see the Appendix for details).

E. Theoretical results

Figure 10 shows computed formation energies of the substitutional and interstitial Mg defects (Mg$_N$, Mg$_{Ga}$, and Mg$_i$), as well as the isolated nitrogen vacancy and its complex with Mg$_{Ga}$ in GaN. The formation energies of these defects indicate that in *p*-type GaN:Mg, the Mg$_{Ga}$ acceptors are likely to be at least partially compensated by several deep donors. Under Ga-rich conditions shown in Fig. 10, the most energetically favorable donor is the V_N defect, suggesting significant concentrations of nitrogen vacancies. The interstitial defect Mg$_i$ and donor-acceptor complex V_N-Mg$_{Ga}$ also have low formation energies in *p*-type GaN, while the Mg$_N$ donor is energetically unfavorable.

The Mg$_{Ga}$ acceptor in GaN is relatively well studied [24], nevertheless some inconsistencies in the reported results still remain. Here we find the Mg$_{Ga}$ thermodynamic transition level at 0.326 eV above the valence band maximum (VBM). PL originating from the radiative recombination of an electron from the conduction band with a hole bound to the Mg$_{Ga}$
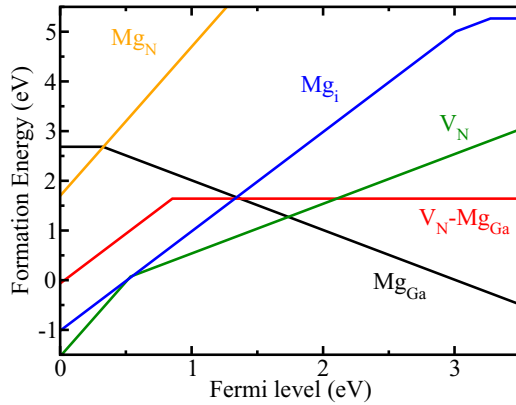
FIG. 10. (Color online) Formation energies of several configurations of the V_N- and Mg-related defects in GaN grown in Ga-rich conditions. Lines with positive slope indicate positively charged defect states (donors), and negative-slope lines indicate negatively charged defects (acceptors).

acceptor has a computed maximum at 3.13 eV and a ZPL at 3.16 eV (Frank-Condon shift of 0.032 eV). These results agree with the position of the UVL band (Fig. 3).

Of the four possible compensating donors shown in Fig. 10, the V_N, $V_N Mg_{Ga}$, and Mg_i defects are more likely to be present in significant concentrations. In p-type GaN, the Mg_i defect has charge 2+ and exhibits two transition levels: the +/2+ level at 0.49 eV below the conduction band minimum (CBM), and the 0/+ level at 0.23 eV below the CBM. Thus, the Mg_i donor can contribute to the compensation of the p-type samples; however, it is unlikely to contribute to the experimentally observed PL. On the other hand, the transition levels of the V_N defect match the experimental data for the GL2 band, as will be shown below.

Figure 11 shows the formation energies and transition levels of the nitrogen vacancy for GaN grown under Ga-rich conditions, when the V_N defect has the lowest formation energy and is expected to be present in significant concentrations. In our calculations, the V_N defect exhibits properties of the negative-U center. Due to large lattice relaxations around the
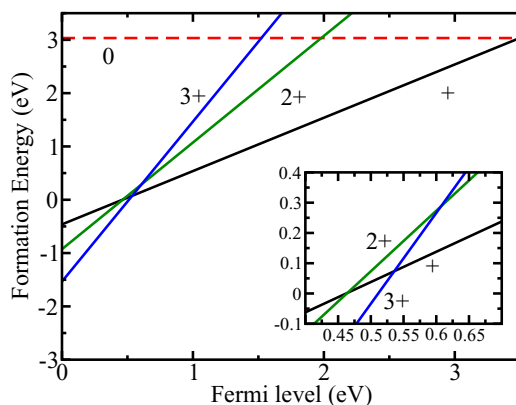

FIG. 11. (Color online) Formation energies of the indicated charged states of the V_N defect in GaN grown under Ga-rich conditions. The inset enlarges the region with the +/2+ and 2+/3+ transition levels, which are at 0.46 and 0.61 eV above the VBM, respectively.

nitrogen vacancy, the 2+ charge state is higher than either the 1+ or 3+ charge states. The outward relaxations of Ga atoms around the vacancy in comparison to the bulk Ga-N bond are 1.12%, 1.45%, 11.33%, and 22.31%, for neutral, 1+, 2+, and 3+ charged states. The resulting thermodynamic transition levels +/2+ and 2+/3+ are at 0.46 and 0.61 eV above the VBM, as shown in Fig. 11. We also find a very shallow 0/+ transition level at 4 meV below the CBM; however, this value is much smaller than the accuracy of our calculations.

The two deep transition levels shown in Fig. 11 allow for two possible optical transitions via the V_N defect. In high-resistivity GaN samples, where the Fermi level is far from the VBM, the lowest energy charge state of the nitrogen vacancy is 1+ (Fig. 11). Therefore, under UV illumination, a photogenerated hole can be captured at the +/2+ level, transferring the V_N defect to the 2+ charge state. (The resonant excitation of an electron from the +/2+ level to the conduction band is unlikely because the corresponding absorption energy is higher than the band gap.) The recombination of an electron from the conduction band with a hole localized at the V_N defect will change its charge from 2+ to 1+ and is expected to cause a PL band with a maximum at 2.24 eV. This value agrees well with the observed maximum of the GL2 band (2.35 eV). The calculated relaxation energy (Frank-Condon shift) of the 1+ charge state following this transition is 0.78 eV, resulting in a ZPL at 3.03 eV, which is in agreement with the ZPL estimates for the GL2 band as discussed in Sec. III D and in the Appendix.

On the other hand, in conductive p-type GaN, where the Fermi level is close to the Mg_{Ga} acceptor level, the V_N defect has charge 3+ in the ground state (Fig. 11). Free electrons can be created by UV illumination, and the capture of a free electron at the 2+/3+ level of the V_N defect is expected to be fast because of the attractive nature of V_N^{3+}. For this transition, the PL maximum is predicted to be at 2.09 eV and the ZPL at 2.88 eV (the relaxation energy is 0.79 eV); however, this is not observed in the measured PL spectra.

Another possible source of PL bands in GaN:Mg grown under Ga-rich conditions is the $V_N Mg_{Ga}$ complex, which is formed by the Coulomb attraction between the V_N^{3+} and Mg_{Ga}^- defects. The details of the energetics and transition levels for the $V_N Mg_{Ga}$ defect are shown in Fig. 12. The formation energy of this complex is roughly 1 eV higher than that of the nitrogen vacancy; however, given the uncertainty of the chemical potentials, it also should be taken into account. The $V_N Mg_{Ga}$ complex forms a negative-U center, which is also due to the strong relaxation of Ga atoms around the nitrogen vacancy. The 1+ state of this defect is always higher than neutral or 2+, resulting in the 0/+ transition level at 0.82 eV and +/2+ transition level at 0.89 eV.

These two levels allow two possible optical transitions through this complex. In p-type samples where the Fermi energy is close to the valence band, the lowest energy charge state of the complex is 2+ (Fig. 12). The emission energy resulting from the recombination of a free electron with a hole localized on the complex (a transition from the 2+ to 1+ state) has been computed to produce a PL band with a maximum at 1.80 eV and a ZPL at 2.6 eV (the relaxation energy is 0.80 eV). In conductive n-type or high-resistivity GaN where the Fermi level is higher than ~0.9 eV from the
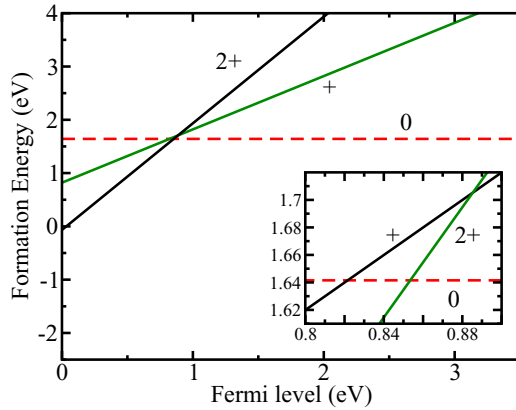
FIG. 12. (Color online) Formation energies of the indicated charged states of the $V_N Mg_{Ga}$ complex in GaN grown under Ga-rich conditions. The inset enlarges the region with the 0/+ and +/2+ transition levels located at 0.82 and 0.89 eV above the VBM, respectively.

VBM, the $V_N Mg_{Ga}$ complex is neutral. Under UV illumination, a photogenerated hole can be captured by the complex, which then becomes positively charged. A transition of an electron from the conduction band to the 0/+ level of the $V_N Mg_{Ga}$ complex is expected to produce a PL band with computed maximum at 1.88 eV and a ZPL at 2.67 eV (the Frank-Condon shift is 0.79 eV). The transitions involving the +/2+ and 0/+ levels of the $V_N Mg_{Ga}$ defect may be related to the RL band, which has a maximum at 1.73 eV in GaN:Mg (Fig. 3).

From the above analysis, we can conclude that, of all the considered defects, only the nitrogen vacancy can contribute to the GL2 band, whereas the Mg_{Ga} acceptor and the $V_N Mg_{Ga}$ complex are expected to be responsible for the UVL and RL bands, respectively.

IV. DISCUSSION

A. Identification of the GL2 band

The properties of the GL2 band with a maximum at 2.35 eV in the studied Mg-doped GaN samples are identical to those in undoped high-resistivity GaN grown under very Ga-rich conditions. Moreover, a very weak GL2 band with the same properties appeared in high-quality undoped freestanding GaN grown by HVPE after the surface was mechanically polished [25]. The quantum efficiency of the GL2 band in Mg-doped GaN samples is the highest among the three groups of samples, which allowed us to study it in more detail and for a wider range of temperatures and excitation intensities.

One of the characteristic features of the GL2 band is a narrow FWHM, which has a strong temperature dependence. From this dependence, the effective phonon energy for the excited state of the related defect was estimated to be $\hbar\Omega_e = 23 \pm 1$ meV—the same value in undoped and Mg-doped GaN samples. Note that the effective phonon energy for the majority of defects in GaN is about twice as large as that for the GL2 band [5,26]. Another characteristic feature of the GL2 band is its thermal quenching at temperatures above 100 K, with an activation energy of about 80–120 meV when it is fit with Eq. (1). This behavior is exhibited in all three types of GaN samples.

The same position, shape, and temperature dependence for the GL2 band in *p*-type GaN:Mg, high-resistivity undoped GaN, and for mechanically polished undoped GaN templates is a strong indication that the GL2 band is caused by the same defect in all of these samples. In the first two cases, very Ga-rich conditions were present during growth. From the candidates for this defect, we exclude defects containing Mg for the following reasons: A strong GL2 band was observed in undoped GaN grown by MBE (where the Mg-related UVL band was not observed at all), and a weak GL2 band was observed even in high-purity bulk GaN templates after their surface was mechanically polished. Therefore, the nitrogen vacancy seems to be an excellent candidate to explain the origin of the GL2 band. Indeed, it is very likely to be formed in Mg-doped GaN samples where the Fermi level is close to the valence band, or in undoped GaN samples grown under very Ga-rich conditions (Fig. 10). As for the bulk GaN templates, the vacancies could be formed along with other structural defects in the near-surface region during the mechanical polishing. This near-surface, defective layer in these samples is thin (about 1 to 2 μm) and can be removed by dry etching [25]. Finally, the transition energy levels of the nitrogen vacancy (calculated in Sec. III E) agree well with the properties of the GL2 band as discussed below.

The activation energy $E_A \approx 80$–120 meV at temperatures below 170 K most probably corresponds to one of the transition levels of the GL2-related defect, which could be the shallow 0/+ level of the V_N defect (Fig. 11). The mechanism of this quenching will be explained in Sec. IV D. At temperatures higher than 180 K, an abrupt and tunable quenching of the GL2 band is observed in the green regions of Mg-doped GaN (Fig. 6), with deduced ionization energy of 0.43 eV. This energy agrees with the activation energy (about 0.4 eV) of the GL2 band that is quenched in the violet regions at $T > 200$ K (Fig. 8). These results are in good agreement with the calculated +/2+ thermodynamic transition level of the V_N defect at 0.46 eV.

B. The abrupt and tunable quenching of GL2 band

In the violet region of Mg-doped GaN (also called the group A samples in Ref. [23]), the GL2 band is very weak. The temperature dependences of both the GL2 and UVL bands are independent of the excitation intensity in this region (Fig. 8); i.e., the thermal quenching is not tunable by excitation intensity. In the green region of Mg-doped GaN (labeled as the group B samples in Ref. [23]), the GL2 band is especially strong. In this region, both the GL2 and UVL bands exhibit abrupt and tunable thermal quenching. An important feature of this behavior is that the abrupt quenching of the UVL and GL2 bands occurs at different temperatures (about 100 and 200 K, respectively), while according to the model suggested previously [10], the abrupt quenching is expected to occur at the same critical temperature T_0 for all PL bands which are caused by the recombination of free electrons with holes bound to different defects. To explain this discrepancy, we need to recall the mechanism of the abrupt and tunable quenching of PL in high-resistivity or *p*-type semiconductors [7,10].

As we discussed in Ref. [10], the abrupt quenching of PL is caused by a sudden redirection of the carrier recombination

flow from a radiative channel (which is responsible for PL) to some nonradiative channel. At low temperatures and under continuous UV illumination, the nonradiative defects are saturated with photogenerated electrons, resulting in a population inversion, an abundance of electrons in the conduction band, and an intense PL signal. The redirection of the carrier recombination flow occurs due to the thermal emission of holes from the radiative defect to the valence band at a characteristic temperature T_0 and the subsequent recapture of these holes by the nonradiative defect. This opens the channel of nonradiative recombination and causes the abrupt quenching of the PL. The characteristic temperature T_0 increases with excitation intensity according to Eq. (4). The quenching is abrupt, and the slope of the quenching is not equal to the activation or ionization energy of any defect. However, the ionization energy of the defect, which triggers the abrupt quenching of PL, can be found from Eq. (4). Simultaneously with the abrupt quenching of PL via this defect, the concentration of free electrons abruptly drops at T_0, and the photoconductivity may switch from n type to p type [7,10,23]. As a result, all PL bands that are caused by transitions of electrons from the conduction band to different defect levels are quenched abruptly at T_0. This was proven in studies of the temperature dependence of photoconductivity in Zn-doped GaN [27].

In contrast to our expectations that all PL bands (related to transitions of electrons from the conduction band to different levels in the band gap) should be quenched simultaneously, the UVL band in the green region of the GaN:Mg samples is quenched abruptly at $T_0 = 80$–100 K (for excitation power densities from 10^{-5} to 10^{-2} W/cm^2), whereas the GL2 band intensity is temperature independent up to 120 K, and its abrupt quenching begins only at $T > 170$ K (Fig. 6). The disparity between the temperature dependences of the UVL and GL2 bands indicates that the electronic transitions in the case of the GL2 band start from an excited state of the same defect, rather than from the conduction band.

The slow and exponential decay of the GL2 emission after pulsed excitation at low temperature and the temperature independence of the PL lifetime between 18 and 100 K also indicate that the transition is internal, and that it does not involve the conduction or valence band. Finally, the position and shape of the GL2 band remain unchanged when the excitation intensity is varied over a wide range, while the UVL band becomes broader and redshifts with decreasing excitation intensity (Fig. 3). The latter can be explained by the presence of potential fluctuations and the tunneling of charge carriers during their recombination. The fact that the GL2 band shape and position do not change with changing excitation intensity supports our assumption that the GL2 band is caused by an internal transition in the V_N defect, because potential fluctuations have no effect on internal transitions. As we have already mentioned in Sec. IV A and as we will discuss in more detail in Sec. IV D, the initial state for the internal transition causing the GL2 band could be the shallow $0/+$ transition level of the V_N defect (Fig. 11).

C. Sharp boundary between the green and violet regions

It has been established from previous studies of Mg-doped GaN grown by MBE that, due to the segregation of Mg at the surface, the polarity may invert from Ga terminated to N terminated [8,28]. This may result in a sudden decrease of Mg incorporation into p-type GaN and an abrupt decrease in the resulting hole concentrations and electrical conductivity [28]. The polarity inversion may occur when the Ga excess is not high enough or if the Mg flux is too high [8,28]. It is therefore likely that the sharp boundary between the green and violet regions in our GaN:Mg samples, and the large difference in the PL intensities of the GL2 and UVL bands in these two regions (Figs. 1 and 2), are caused by a sudden polarity inversion. The resulting drop in concentration of the Mg acceptors leads to an abrupt shift of the Fermi level from the shallow Mg_{Ga} acceptor level to the deep level of the dominant compensating donor. The main candidates for these donors and the expected positions of the Fermi level in our GaN:Mg samples can be suggested based on the theoretical calculations presented in Sec. III E and summarized in Fig. 10.

The doping of GaN with Mg introduces the Mg_{Ga} acceptor with the $-/0$ level at about 0.2 eV above the valence band. In spite of the relatively high formation energy of the Mg_{Ga} acceptors in p-type GaN:Mg obtained in Ga-rich conditions (Fig. 10), highly nonequilibrium conditions during the MBE growth can provide significant Mg concentrations. For example, decreasing the growth temperature from 710 to 650 °C may lead to an increase in the Mg concentration from 10^{18} to 10^{20} cm^{-3} (as demonstrated in Ref. [28]). However, at the same time when the Fermi level is close to the valence band, the formation of compensating donors, such as V_N, $V_N Mg_{Ga}$, and Mg_i, is very likely, especially in Ga-rich conditions (Fig. 10). The $2+/3+$ and $+/2+$ transition levels of the V_N defect (which is presumably responsible for the GL2 band) are located at about 0.5 eV above the top of the valence band. The $+/2+$ and $0/+$ transition levels of the $V_N Mg_{Ga}$ complex are higher, at about 0.9 eV above the top of the valence band. The $+/2+$ and $0/+$ levels of the Mg_i defect are significantly higher, around 3.30 to 3.27 eV above the VBM. From the dependence of the GL2 band intensity on excitation intensity (Fig. 4), the estimated concentration of nitrogen vacancies is relatively low, about 10^{16} cm^{-3}. (This may indicate that the very low computed formation energy of V_N is probably overestimated). Since the concentration of V_N is most likely low, the $V_N Mg_{Ga}$ complexes and the Mg_i defects (both are donors) could become the dominant compensating donors and cause partial or complete compensation in conductive p-type or high-resistivity GaN:Mg. In the following explanations of the GL2 band, we will assume for certainty that the Fermi level in the violet regions is near the shallow Mg_{Ga} acceptor level, while in the green region, the Fermi level is stabilized by the $V_N Mg_{Ga}$ donor level. The transition from the violet to green region results in the abrupt shift of the Fermi level from 0.2 to 0.9 eV above the valence band due to the switch of polarity and the sudden drop in Mg_{Ga} concentration, which leads to the abrupt change of the V_N defect charge state from $3+$ to $1+$.

D. Mechanism of the GL2 band

To explain the extensive experimental data, we suggest the following mechanism for the GL2 band in GaN (Fig. 13). In dark, all the V_N centers are in the $1+$ charge state for high-resistivity GaN. Under UV illumination, the absorbed photons
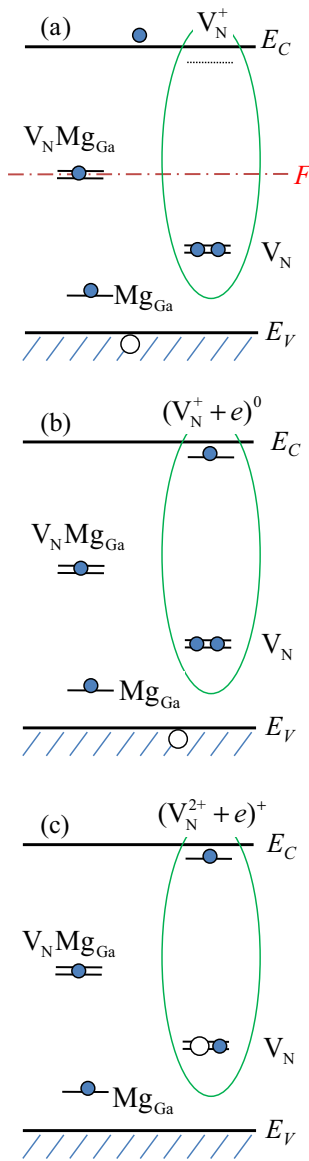
FIG. 13. (Color online) Band diagrams and schematic explanation of the processes in high-resistivity GaN:Mg. (a) The Fermi level in dark is stabilized by a deep donor $V_N Mg_{Ga}$ and lies close to its transition level. The nitrogen vacancy in dark appears as the V_N^+ center. Absorption of a photon with above-bandgap energy creates a free electron (filled circle) and a free hole (empty circle). (b) The electron is captured by the nitrogen vacancy and remains weakly bound to it. The capture of this electron does not distort the atomic configuration around V_N^+, because the electron wave function is weakly localized. (c) A free hole is captured by the nitrogen vacancy and recombines with one of the strongly localized electrons. This is an excited state where the weakly localized electron has little effect on the atomic arrangement for V_N, which in this state is very similar to that of a pure V_N^{2+} center. The system remains in the excited state for about 0.3 ms and then collapses to the ground state shown in (a). This happens by an internal transition: The weakly bound electron falls to the localized state and emits a photon.

generate electron-hole pairs [Fig. 13(a)]. First, an electron is captured by the $0/+$ level of the V_N^+ center (in less than 1 ns), converting it to a V_N^0 center. The $0/+$ level is close to the conduction band (about 0.1 eV below the CBM), and

the electron is weakly localized. Since this electron does not distort the atomic configuration, we can regard the defect as V_N^+ plus a weakly localized electron [Fig. 13(b)].

Next, a free hole is captured by the defect. But, instead of recombining with the weakly localized electron, it recombines with one of the electrons at the localized orbitals of the V_N center. As a result, the center becomes V_N^{2+} plus a weakly localized electron [Fig. 13(c)]. The distortion of the defect is not affected by the weakly localized electron, and the adiabatic potential for this defect should have the same minimum as a pure V_N^{2+} center.

The last step is the internal transition: The weakly localized electron collapses to the localized orbital, and the center ends in the V_N^+ state. The characteristic time of this internal transition is about 0.3 ms according to time-resolved PL data. During this time, two processes may happen that will prevent recombination: (i) The weakly localized electron can be ionized at $T > 80$ K (with an activation energy of 0.1 eV) and leave the defect, converting the defect into the V_N^{2+} state which then may capture an electron to the shallow excited state again or remain in this charge state for a long time. (ii) At higher temperatures ($T > 180$ K), the hole can be thermally emitted to the valence band, and the defect converts from the V_N^{2+} to the V_N^+ state. If the hole escapes and recombines via other channels, the GL2 band will be thermally quenched with the activation energy determined by the position of the $+/2+$ level above the valence band.

The thermal emission of holes causes a tunable quenching of the GL2 band in high-resistivity GaN:Mg, because at low temperatures the population inversion is dictated by some nonradiative centers, similar to the case of the blue luminescence band in high-resistivity GaN:Zn [10]. Then, the quenching is abrupt, and the related "activation" energy has no relation to the ionization energy of the V_N defect. However, in conductive p-type GaN:Mg, the quenching is not tunable, and the activation energy of the quenching is equal to the ionization energy of the V_N defect. Note that the quenching of the GL2 band at temperatures between 100 and 180 K with an activation energy of about 0.1 eV is expected to be the same (not tunable) in both types of samples (high-resistivity and conductive p-type), because it is caused by the thermal emission of electrons to the conduction band, not holes to the valence band. This agrees with the experimental observations.

E. Other defects and PL bands in Mg-doped GaN

1. The UVL, BL, and RL bands in Mg-doped GaN

In the literature, the most common PL bands in Mg-doped GaN are the UVL band with a maximum at about 3.25 eV and the blue luminescence (BL) band with a maximum at about 2.8 eV. Observations of the GL2 band in GaN are rare, and we explain the strong GL2 band in our samples by the Ga-rich conditions during MBE growth that result in the formation of relatively high concentrations of V_N and other compensating donors. It also appears that the GL2 band is not commonly observed in Mg-doped GaN, because it is masked by a much stronger BL band, which is usually very strong in Mg-doped GaN grown by metal-organic chemical-vapor deposition (MOCVD). Finally, the GL2 band saturates with increasing excitation intensity (Fig. 4), and very low excitation

intensities are needed for its observation, which is not typical for experimental conditions used by a majority of researchers.

The BL band in Mg-doped GaN commonly appears in MOCVD-grown GaN heavily doped with Mg. It can be greatly enhanced by thermal annealing at temperatures 600–800 °C [29]. The BL band is attributed to transitions from a deep donor ($\sim$0.4 eV below the conduction band) to the shallow Mg_{Ga} acceptor [5,18,30–33]. Such an attribution explains a very large shift of the BL band with increasing excitation intensity (from $\sim$2.7 to $\sim$3.0 eV), along with other properties of this band [18]. An alternative model—according to which the BL band is caused by transitions of electrons from the conduction band to the Mg_{Ga} acceptor [24]—cannot explain the large shift of the BL band maximum and the fact that in some Mg-doped GaN samples the BL band is not observed at all (such as in Fig. 3). According to extensive experimental data, the transitions of electrons from the conduction band to the Mg_{Ga} acceptor are responsible for the UVL band [5,30]. In the literature, a deep donor with an energy of about 0.4 eV below the conduction band, which is involved in the BL band, is sometimes attributed to the $V_N Mg_{Ga}$ complex [5]. However, our calculations and experimental results for Mg-doped GaN grown in Ga-rich conditions by MBE suggest that the $V_N Mg_{Ga}$ donor has no relation to the BL band. Moreover, the BL band is greatly enhanced by thermal annealing, whereas the concentration of the $V_N Mg_{Ga}$ complexes significantly decreases after annealing at $T > 500$ °C [34,35]. Since the BL band is commonly observed in GaN:Mg grown by MOCVD and rarely observed in the MBE-grown GaN:Mg [5], one may expect that the deep donor involved in the BL band contains hydrogen as a part of the defect. Such an assumption is supported by the annealing studies in H plasma, according to which the BL band is greatly enhanced by remote plasma treatment, with plasma containing atomic hydrogen [32].

Finally, according to our calculations and the results of Ref. [2], the $V_N Mg_{Ga}$ complex may be responsible for the RL band, which has a maximum at 1.73 eV. However, in our GaN:Mg samples, the RL band is much weaker than the GL2 band, and it saturates at very low excitation intensities, indicating that there might be alternative explanations for the RL band.

2. The YL and GL2 bands in Mg-doped GaN

The YL band with a maximum at 2.2–2.3 eV is sometimes observed in Mg-doped GaN [4,36–39]. We clearly distinguish this band from the GL2 band with a maximum at 2.35 eV studied in the current work. The former is possibly caused by a contamination of the samples with carbon [17,40]. Careful experiments should be conducted on the samples containing the YL band in Mg-doped GaN in order to confirm the conductivity type and to establish the origin of the related transitions. Usually, when the YL band is observed in Mg-doped GaN, these samples appear to be *n* type [37–39]. Sometimes, the authors discuss the defect-related band as the YL band, whereas in fact it is the same GL2 band as the one studied in this work. For example, Ronning, Carlson, and Davis [41] reported on defects in GaN implanted with Mg and identified the PL band with a maximum at 2.35 eV as the YL band. However, the position and shape of this PL band

(the bandwidth at the level of 0.1 from the maximum is about 0.4 eV) are identical to those for the GL2 band shown in Fig. 9 and are quite different from those for the YL band in GaN [5].

In several works on Mg-implanted GaN, the UVL band and a green luminescence band were observed [42–44]. The position and shape of the dominant green band are nearly identical to those of the GL2 band, yet detailed investigations were not conducted in these works. The samples were grown by HVPE [43], or MOCVD [41,44], and after the Mg implantation and rapid annealing, no *p*-type behavior could be obtained because of compensation with some donors. The BL band was not observed in these samples, which agrees with our assumption that the BL band is related to defects containing hydrogen.

V. CONCLUSIONS

A strong green luminescence band with a maximum at 2.35 eV is observed in MBE-grown, high-resistivity GaN doped with Mg. This band, labeled GL2, was previously observed in undoped, high-resistivity GaN grown under very Ga-rich conditions and also in HVPE-grown, bulk GaN templates after mechanical polishing of their surfaces. Our first-principles calculations predict the formation of three donor defects in Mg-doped GaN: a nitrogen vacancy, interstitial Mg, and the nitrogen-vacancy–magnesium complex. The GL2 band is attributed to internal transitions within the V_N donor. In the internal transition causing the GL2 band, an electron from a weakly localized state of the V_N defect recombines with a strongly localized hole. While the total charge of the defect does not change in this transition, the atomic configuration changes from the V_N^{2+} to the V_N^+ state. A simple, one-dimensional configuration-coordinate diagram explains the slightly asymmetric shape of the GL2 band and predicts that the zero-phonon line for this transition is close to 3 eV. The Huang-Rhys factors for the ground and excited states of the nitrogen vacancy (V_N^+ and V_N^{2+}, respectively) are higher than 20.

In experiment, we observed a sharp change of PL properties when the laser beam passed from the high-resistivity region (labeled as "green") to a conductive *p*-type region (labeled "violet"). The sharp change is explained by an abrupt shift of the Fermi level when the material conductivity changes from high resistivity to conductive *p* type, presumably due to a polarity inversion. In this transition, the charge state of the nitrogen vacancy changes from 1+ to 3+. It appears that only the V_N^+ state produces intense PL, because photogenerated electrons are quickly captured by this state and after 0.3 ms recombine with a strongly localized hole to produce the GL2 band. Other transitions are most likely nonradiative.

In the green regions of GaN:Mg, the thermal quenching of the GL2 and UVL bands is tunable; i.e., the characteristic temperature of this quenching shifts to higher energies with increasing excitation intensity. In the violet regions, no tunable quenching can be observed. We explain such different behaviors with the assumption that a significant concentration of the Mg acceptors in *p*-type GaN remain filled with holes in dark, and the conditions of the population inversion (which is responsible for the tunable quenching effect) are difficult to achieve.

ACKNOWLEDGMENTS

APPENDIX: CONFIGURATION-COORDINATE MODEL FOR THE NITROGEN VACANCY IN GaN

In order to explain the shape of the GL2 band and obtain phenomenological parameters of the related defect, we constructed a one-dimensional configuration-coordinate diagram shown in Fig. 14. The adiabatic potentials are parabolas, and the diagram describes the total energy of the defect system (the energy of atoms plus the energy of electrons). The ground state of the defect (potential 1) corresponds to the $1+$ charge state of the V_N defect. Its energy varies in one-dimensional space as $U_g = \frac{1}{2}K_g q^2$, where the coefficient K_g is analogous to the spring constant in the problem of a simple harmonic oscillator, and q is the generalized coordinate. The coefficient K_g can be presented as $K_g = m_g \Omega_g^2$, where m_g is the effective mass of the oscillating system involving our defect in the ground state, and Ω_g is the effective phonon frequency in this state [45]. After a photon is absorbed, a hole and an electron appear in the valence and conduction bands, respectively, and the energy of the system increases by $E_g = 3.5$ eV [potential 2 in Fig. 14, which corresponds to the band diagram shown in Fig. 13(a)]. Due to the Coulomb attraction by the V_N^+ defect, a free electron is captured quickly and forms a weakly localized state about 0.1 eV below the conduction band minimum. Since the electron is weakly localized, the distortion of the system does not change (same position and shape of the adiabatic potential minimum), but the total energy of the system decreases [potential 2* in Fig. 14, which corresponds to the band diagram shown in Fig. 13(b)]. Then, a hole is captured by the V_N center at one of the valence electron orbitals, and the center becomes doubly charged. This bound hole causes the distortion of the atomic arrangement, and the system relaxes to its equilibrium minimum [potential 3 in Fig. 14, which corresponds to the band diagram shown in Fig. 13(c)] by emitting many local phonons. The recombination of the weakly bound electron with one of the localized holes is an internal transition, with a characteristic waiting time of 250–300 μs. The energy of the system in the excited state (potential 3) is $K_e = m_e \Omega_e^2$, where m_e is not necessarily equal to m_g, and Ω_e is the effective phonon frequency in the excited state. The Huang-Rhys factors for the ground state S_g and the excited state S_e indicate the mean number of absorbed and emitted phonons; i.e.,

$$\frac{1}{2}K_g q_0^2 = S_g \hbar \Omega_g \tag{A1}$$

and

$$\frac{1}{2}K_e q_0^2 = S_e \hbar \Omega_e. \tag{A2}$$

From Eqs. (A1) and (A2), we can obtain the relation between the Huang-Rhys factors and the phonon energies in the ground and excited states:

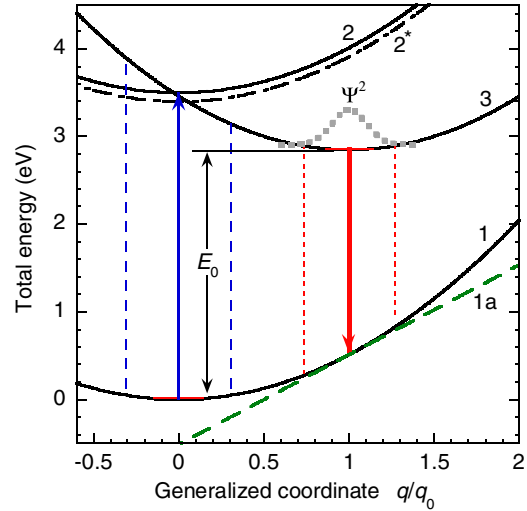$$\frac{S_e}{S_g} = \frac{m_e \hbar \Omega_e}{m_g \hbar \Omega_g}. \tag{A3}$$

FIG. 14. (Color online) Adiabatic potentials for the V_N defect. The potential 1 represents the total energy of the system in the ground state when the V_N defect is in the $1+$ state. The potential 2 is the same system plus a free electron in the conduction band and a free hole in the valence band. The vertical upward arrow indicates the excitation process, and the dashed vertical lines on both sides of this arrow indicate the transitions for which the PL excitation intensity decreases by a factor of 100 from its maximum. The potential 2* corresponds to the capture of a weakly localized electron by the V_N^+ defect. The potential 2* is identical to the potential 2 but shifted downwards by 0.1 eV. The potential 3 corresponds to the V_N defect in the $2+$ state (a bound hole plus the weakly localized electron). The transition from the minimum of potential 2* to the minimum of potential 3 corresponds to the capture of a hole by the V_N defect and the emission of a large number of phonons (about 26). The shift of the excited state minimum relative to the ground state minimum by $q = q_0$ describes the lattice relaxation. The dotted, bell-shaped curve in the minimum of state 3 indicates the square of the wave function of the defect in the excited state. The vertical downward arrow from state 3 to state 1 indicates a transition causing the emission of a photon with energy corresponding to the maximum of the GL2 band. The thin dotted lines on both sides of this arrow outline the range where the probability function is higher than 0.01. The projections of the intersections of these dotted lines with potential 1 on the vertical axis give the width of the GL2 band at the level 0.01 from its maximum. The straight line 1a is a tangent to the parabola 1 in point $q = q_0$. If the potential of the ground state between the dotted vertical lines was a straight line such as line 1a, the shape of the GL2 band would be a perfect Gaussian curve as is shown with a thick dashed line in Fig. 9. Because of the parabolic shape of potential 1, the line shape of the GL2 band is slightly asymmetrical (Fig. 9). After the emission of a photon, the system relaxes to the minimum of the ground state by emitting multiple phonons. The average number of emitted phonons is about 24.

Finally, the Stokes shift in the ground state is

$$\hbar \Omega_g S_g = (E_0 - \hbar \omega_{max}) + \frac{1}{2}\hbar \Omega_g \approx (E_0 - \hbar \omega_{max}) + \frac{1}{2}\hbar \Omega_e, \tag{A4}$$

where E_0 is the energy of the ZPL.

The energy of the emitted photon corresponding to an arbitrary value of q and to the maximum of the GL2 band

(the downward arrow in Fig. 14) is

$$\hbar\omega = E_0 + \tfrac{1}{2}\hbar\Omega_e - \tfrac{1}{2}K_g q^2 \qquad (A5)$$

and

$$\hbar\omega_{\max} = E_0 + \tfrac{1}{2}\hbar\Omega_e - \tfrac{1}{2}K_g q_0^2, \qquad (A6)$$

respectively. The probability function at the lowest level ($n = 0$) of the excited state 3 is

$$\Psi^2 = A \, \exp\left(-\frac{K_e(q-q_0)^2}{\hbar\Omega_e}\right) = A \, \exp\left[-2S_e\left(\frac{q}{q_0}-1\right)^2\right], \qquad (A7)$$

where A is a constant. The dependence of the PL intensity on photon energy can be obtained by substituting the expressions for q and q_0 from Eqs. (A5) and (A6) into Eq. (A7) with the result given by

$$I^{\mathrm{PL}} \propto \exp\left[-2S_e\left(\sqrt{\frac{E_0 + 0.5\hbar\Omega_e - \hbar\omega}{E_0 + 0.5\hbar\Omega_e - \hbar\omega_{\max}}} - 1\right)^2\right]. \qquad (A8)$$

This is the same as Eq. (8).

In the case of very strong electron-phonon coupling, when the curvature of the parabola decreases and approaches a straight line, the potential 1 near the point $q = q_0$ can be replaced with a tangent (line 1a) in Fig. 14. Then, the dependence of the photon energy on q is

$$\hbar\omega = E_0 + \frac{1}{2}\hbar\Omega_e + S_g\hbar\Omega_g\left(2\frac{q}{q_0}-1\right), \qquad (A9)$$

and the spectral dependence of the PL intensity becomes

$$I^{\mathrm{PL}} \propto \Psi^2 = A \, \exp\left(-\frac{(\hbar\omega - \hbar\omega_{\max})^2}{2\sigma^2}\right), \qquad (A10)$$

where $\sigma = S_g\hbar\Omega_g/\sqrt{S_e}$. Then the FWHM of the PL band at zero temperature, $W(0)$, is

$$W(0) = \sqrt{8\ln 2}\frac{S_g\hbar\Omega_g}{\sqrt{S_e}}. \qquad (A11)$$

This result is identical to the commonly used expression for $W(0)$ [see Eq. (26) in Ref. [5]]. However, we emphasize that it is valid only for defect-related PL bands with a symmetrical Gaussian shape. For a general case, Eq. (A8) should be used.

From the fit of the experimental shape of the GL2 band with Eq. (A8), by using $\hbar\omega_{\max} = 2.35$ eV and $\hbar\Omega_e = 23$ meV, we obtained $E_0 = 2.85$ eV and $S_e = 26.5$ (Fig. 9). Since the PL excitation spectrum for the GL2 band does not show any PL excitation band below the band gap, the shape and position of the PL excitation band is unknown. However, the parameters S_g and $\hbar\Omega_g$ still can be estimated by solving the system of Eqs. (A3), (A4), and (A11), with the assumption that $m_e = m_g$. Then, one can obtain $S_g = 24.3$ and $\hbar\Omega_g = 21.1$ eV. All these parameters were used to construct the configuration-coordinate diagram shown in Fig. 14. This diagram explains well the GL2 band spectrum in Fig. 9. Note that the asymmetry of the GL2 band is evident only when its shape is analyzed over a wide range (two orders of magnitude). If the PL band shape is analyzed only above half of its maximum, the asymmetry is not visible within the experimental error, and the uncertainty
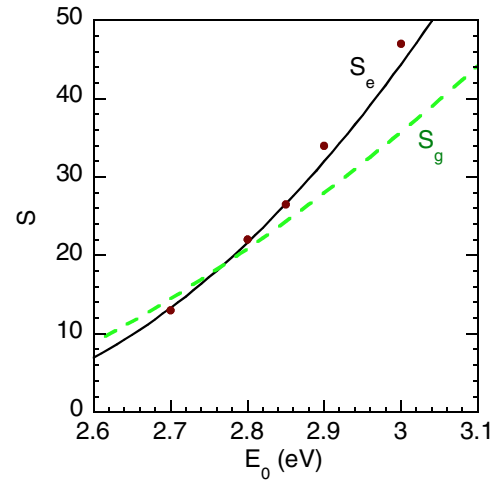

FIG. 15. (Color online) Possible values of parameters S_e and S_g as a function of possible values of E_0 for a PL band having a maximum at 2.35 eV and the FWHM of 0.23 eV at low temperature. The solid and dashed lines are the values of S_e and S_g, respectively, obtained from a solution of the system of Eqs. (A3), (A4), and (A10) for the range of the parameter E_0 from 2.6 to 3.1 eV with the following fixed parameters: $W(0) = 230$ meV, $\hbar\omega_{\max} = 2.35$ eV, $\hbar\Omega_e = 23$ meV, and $m_e = m_g$. The filled symbols are examples of possible values of S_e and E_0 obtained from the fit of the GL2 line shape with Eq. (A8) in a wider range.

of the model parameters increases substantially. Figure 15 shows the values of the parameters S_e and S_g that satisfy Eqs. (A3), (A4), and (A11) for the given $W(0) = 230$ meV and $\hbar\Omega_e = 23$ meV.

The fact that the GL2 band could not be excited resonantly with energies of incident photons lower than 3.25 eV (Ref. [5]) is in agreement with the configuration-coordinate diagram shown in Fig. 14. Accordingly, the intensity of the PL excitation band at 3.25 eV is expected to be only 0.01 from its maximum (a dashed vertical line to the right from the upward arrow). This means that it is unlikely that $E_0 < 2.85$. However, the values in the range of 2.85–3.0 eV are acceptable (Fig. 15), with the value $E_0 = 2.85$ eV providing the best agreement between the shapes of the GL2 band obtained experimentally and calculated from the one-dimensional configuration-coordinate diagram (Fig. 9).

The above-found vibrational parameters of the defect responsible for the GL2 band agree with the parameters for the nitrogen vacancy calculated by Alkauskas *et al.* [3]. These authors predicted that the Huang-Rhys factors are very large, and the effective phonon energies are small for deep donors such as the V_N defect in GaN. From first-principles calculations, the ZPL for the V_N defect is expected to be at 3 eV, far from the high-energy side of the defect-related PL band. Our PL excitation results for the GL2 band (Ref. [5]) and the detailed analysis of the shape of the GL2 band (Figs. 9 and 14) suggest that E_0 is equal to or higher than 2.85 eV, but not higher than $\sim$3.0 eV. The effective phonon energies for the V_N defect are predicted from first-principles calculations to be about 21–23 meV, and the Huang-Rhys factors to be about 35 [3]. From analysis of the experimental data for the GL2 band, we have found that the effective phonon energies for the related defect are about 18–23 meV, and the Huang-Rhys

factors are close to 25 or higher (up to about 40; see Fig. 15). Note, however, that the parameters in Ref. [3] were found for the transitions between the 3+ and 2+ charge states of the V_N

defect, while in our model we predict that the GL2 band is caused by transitions between the 2+ and 1+ states of the V_N defect.

[1] C. G. Van de Walle and J. Neugebauer, J. Appl. Phys. **95**, 3851 (2004).

[2] Q. Yan, A. Janotti, M. Scheffler, and C. G. Van de Walle, Appl. Phys. Lett. **100**, 142110 (2012).

[3] A. Alkauskas, J. L. Lyons, D. Steiauf, and C. G. Van de Walle, Phys. Rev. Lett. **109**, 267401 (2012).

[4] G. Salviati, N. Armani, C. Zanotti-Fregonara, E. Gombia, M. Albrecht, H. P. Strunk, M. Mayer, M. Kamp, and A. Gasparotto, MRS Internet J. Nitride Semicond. Res. **5S1**, W11.50 (2000).

[5] M. A. Reshchikov and H. Morkoç, J. Appl. Phys. **97**, 061301 (2005).

[6] M. A. Reshchikov, R. Molnar, and H. Morkoç, Mat. Res. Soc. Symp. Proc. **680E**, E5.6 (2001).

[7] M. A. Reshchikov, J. Appl. Phys. **115**, 012010 (2014).

[8] D. S. Green, E. Haus, F. Wu, L. Chen, and J. S. Speck, J. Vac. Sci. Technol. B **21**, 1804 (2003).

[9] B. Heying, R. Averbeck, L. F. Chen, E. Haus, H. Riechert and J. S. Speck, J. Appl. Phys. **88**, 1855 (2000).

[10] M. A. Reshchikov, A. A. Kvasov, M. F. Bishop, T. McMullen, A. Usikov, V. Soukhoveev, and V. A. Dmitriev, Phys. Rev. B **84**, 075212 (2011).

[11] M. A. Reshchikov, M. A. Foussekis, J. D. McNamara, A. Behrends, A. Bakin, and A. Waag, J. Appl. Phys. **111**, 073106 (2012).

[12] J. Heyd, G. E. Scuseria, and M. Ernzerhof, J. Chem. Phys. **118**, 8207 (2003).

[13] G. Kresse and J. Furthmüller, Phys. Rev. B **54**, 11169 (1996).

[14] D. O. Demchenko and M. A. Reshchikov, Phys. Rev. B **88**, 115204 (2013).

[15] H. Morkoç, *Handbook of Nitride Semiconductors and Devices* (Wiley, New York, 2008), Vols. 1–3.

[16] S. Lany and A. Zunger, Phys. Rev. B **78**, 235104 (2008).

[17] D. O. Demchenko, I. C. Diallo, and M. A. Reshchikov, Phys. Rev. Lett. **110**, 087404 (2013).

[18] M. A. Reshchikov, G.-C. Yi, and B. W. Wessels, Phys. Rev. B **59**, 13176 (1999).

[19] M. A. Reshchikov, Appl. Phys. Lett. **88**, 202104 (2006).

[20] M. A. Reshchikov, in *Internal Quantum Efficiency of Photoluminescence in Wide-Bandgap Semiconductors*, edited by M. A. Case and B. C. Stout, Photoluminescence: Applications, Types and Efficacy (Nova Science Publishers, Inc., New York, 2012), pp. 53–120.

[21] J. F. Muth, J. H. Lee, I. K. Shmagin, R. M. Kolbas, H. C. Casey, B. P. Keller, U. K. Mishra, and S. P. DenBaars, Appl. Phys. Lett. **71**, 2572 (1997).

[22] M. A. Reshchikov, Phys. Rev. B **85**, 245203 (2012).

[23] M. A. Reshchikov, J. D. McNamara, S. Fernández-Garrido, and R. Calarco, Phys. Rev. B **87**, 115205 (2013).

[24] J. L. Lyons, A. Janotti, and C. G. Van de Walle, Phys. Rev. Lett. **108**, 156403 (2012).

[25] J. D. McNamara, M. A. Foussekis, A. A. Baski, X. Li, V. Avrutin, H. Morkoç, J. H. Leach, T. Paskova, K. Udwary, E. Preble, and M. A. Reshchikov, Phys. Status Solidi C **10**, 536 (2013).

[26] M. A. Reshchikov, *Carrier-capture characteristics of point defects in GaN and ZnO*, AIP Conf. Proc. 1583 (AIP, Melville, NY, 2014), p. 127.

[27] M. A. Reshchikov, *Temperature dependence of photoconductivity in Zn-doped GaN*, AIP Conf. Proc. 1583 (AIP, Melville, NY, 2014), p. 292.

[28] A. Feduniewicz, C. Skierbiszewski, M. Siekacz, Z. R. Wasilewski, I. Sproule, S. Grzanka, R. Jakieła, J. Borysiuk, G. Kamler, E. Litwin-Staszewska, R. Czernecki, M. Boćkowski, and S. Porowski, J. Cryst. Growth **278**, 443 (2005).

[29] S. Nakamura and G. Fosol, *The Blue Laser Diode* (Springer, Berlin, 1998).

[30] U. Kaufmann, M. Kunzer, H. Obloh, M. Maier, Ch. Manz, A. Ramakrishnan, and B. Santic, Phys. Rev. B **59**, 5561 (1999).

[31] B. Monemar, P. P. Paskov, G. Pozina, C. Hemmingsson, J. P. Bergman, S. Khromov, V. N. Izyumskaya, A. Avrutin, X. Li, H. Morkoç, H. Amano, M. Iwaya, and I. Akasaki, J. Appl. Phys. **115**, 053507 (2014).

[32] Y. Kamiura, M. Kaneshiro, J. Tamura, T. Ishiyama, Y. Yamashita, T. Mitani, and T. Mukai, Jpn. J. Appl. Phys. **44**, L926 (2005).

[33] H. Teisseyre, T. Suski, P. Perlin, I. Grzegory, M. Leszczynski, M. Bockwoski, S. Porowski, J. A. Freitas, R. L. Henry, A. E. Wickenden, and D. D. Koleske, Phys. Rev. B **62**, 10151 (2000).

[34] S. Hautakangas, K. Saarinen, L. Liszkay, J. A. Freitas, Jr., and R. L. Henry, Phys. Rev. B **72**, 165303 (2005).

[35] S. Hautakangas, V. Ranki, I. Makkonen, M. J. Puska, K. Saarinen, L. Liszkay, D. Seghier, H. P. Gislason, J. A. Freitas, Jr., R. L. Henry, X. Xu, and D. C. Look, Physica B **376–377**, 424 (2006).

[36] O. Gelhausen, H. N. Klein, M. R. Phillips, and E. M. Goldys, Appl. Phys. Lett. **83**, 3293 (2003).

[37] M. W. Bayerl, M. S. Brandt, O. Ambacher, M. Stutzmann, E. R. Glaser, R. L. Henry, A. E. Wickenden, D. D. Koleske, T. Suski, I. Grzegory, and S. Porowski, Phys. Rev. B **63**, 125203 (2001).

[38] B. Monemar, P. P. Paskov, J. P. Bergman, A. A. Toropov, T. V. Shubina, S. Figge, T. Paskova, D. Hommel, A. Usui, M. Iwaya, S. Kamiyama, H. Amano, and I. Akasaki, Mater. Sci. Semicond. Process. **9**, 168 (2006).

[39] J. K. Sheu, Y. K. Su, G. C. Chi, B. J. Pong, C. Y. Chen, C. N. Huang, and W. C. Chen, J. Appl. Phys. **84**, 4590 (1998).

[40] J. L. Lyons, A. Janotti, and C. G. Van de Walle, Appl. Phys. Lett. **97**, 152108 (2010).

[41] C. Ronning, E. P. Carlson, and R. F. Davis, Phys. Rep. **351**, 349 (2001).

[42] J. A. Fellows, Y. K. Yeo, R. L. Hengehold, and L. Krasnobaev, Mater. Res. Soc. Symp. Proc. **680E**, E7.1 (2001).

[43] B. J. Skromme and G. L. Martinez, MRS Internet J. Nitride Semicond. Res. **5S1**, W9.8 (2000).

[44] G.-C. Chi, B. J. Pong, C. J. Pan, Y. C. Tang, and C. H. Lee, Mater. Res. Soc. Symp. Proc. **482**, 1027 (1998).

[45] K. K. Rebane, *Impurity Spectra of Solids* (Plenum, New York, 1970).